Materials Characterization 146 (2018) 91–100

Contents lists available at ScienceDirect

Materials Characterization

journal homepage: www.elsevier.com/locate/matchar

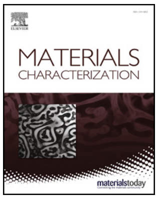

A detailed study of the microstructure and thermal stability of typical SiC fibers

Yong Zhang[a], Cuilan Wu[a,*], Yingde Wang[b], Jianghua Chen[a], Yang Qiu[c], Xiubo Yang[a], Yanzi Gou[b,*]

[a] *Center for High Resolution Electron Microscopy, College of Materials Science and Engineering, Hunan University, Changsha 410082, China*
[b] *Science and Technology on Advanced Ceramic Fibers and Composites Laboratory, National University of Defense Technology, Changsha 410073, China*
[c] *Pico Center, Materials Characterization and Preparation Center, Southern University of Science and Technology, Shenzhen 518055, China*

ARTICLE INFO

Keywords:
SiC fibers
Graphite
Electron microscopy
Microstructure
Thermal stability

ABSTRACT

Continuous SiC fibers have attracted increasing research interest for their significant application in aerospace and nuclear energy. Control of inhomogeneity and decrement of defects are crucial for improving the mechanical and high-temperature performance of SiC fibers. Thus an understanding of fine and detailed microstructural and microchemical distribution of SiC fibers is urgently needed. In the present work, the cross-sectional phase distributions, morphologies and defects of amorphous, non-stoichiometric and near-stoichiometric SiC fibers were well characterized. From surface to core, the amorphous and non-stoichiometric fibers exhibited uniform microstructures, but a gradient change along the radial direction was observed in the near-stoichiometric fiber. Nanosized SiC and turbostratic carbon (2–4 nm) were randomly distributed inside the amorphous fiber. A large amount of graphite surrounding SiC grains appears in the non-stoichiometric fiber which possess low strength and weak thermal stability. The near-stoichiometric fiber has transgranular fracturing, high strength and favorable thermal stability, and the graphite planes are turbostratic inside the fiber but straight on the surface. The results of both energy-dispersive X-ray spectrometry measurements and first-principles calculations demonstrate that Al atoms can occupy Si sites in the SiC grains. Our findings offer fine understanding for fabricating SiC fibers with superior properties.

1. Introduction

Due to high tensile strength, high elastic modulus, excellent thermal stability and good oxidation resistance, continuous SiC fibers prepared via polymer-derived methods have attracted great interest [1–3]. SiC fibers can serve as a reinforce material in ceramic or metal matrices to form ceramic (metal) matrix composites, such as SiC_f/C, SiC_f/SiC and SiC_f/Al, which have wide application in the field of aerospace, nuclear energy, etc. [4–8]. To date, much attention has been paid to the polymeric precursor synthesis, sintering conditions and microstructural characterizations to optimize the mechanical and thermal properties of the SiC fibers [9–18]. The precursor polyaluminocarbosilane (PACS), which contains aluminum (Al), was synthesized by the reaction between polycarbosilane (PCS) and aluminum (III) acetylacetonate ($Al(Ac)_3$) at ~300 °C [19,20]. This type of SiC fiber derived from PACS has high mechanical properties and excellent thermal stability (even at temperatures above 1900 °C) [21]. In general, the PACS-derived SiC fibers consist of SiC grains (grain size ~200 nm), free carbon phase (mainly in the form of graphite), and a small amount of oxygen (~0.5 wt%) and aluminum (< 1 wt%). Considering their high-temperature resistance performance, the near-stoichiometric SiC fibers with a C/Si atomic ratio slightly larger than unity are possibly the best reinforcements to date [11].

It is well known that the fabrication of SiC fibers involve a series of complex processes, including precursor synthesis, melt-spinning, air curing, pyrolysis and sintering, which usually produce various inhomogeneity in composition and microstructure, thus have a remarkable influence on the property of the fibers [22]. For example, the residual free carbon has detrimental effects on the mechanical properties, which is strongly correlated to the presence of oxygen introduced during the curing process [15,23]. At the same time, pores and extra defects may easily form due to gases released during the sintering process [22]. Therefore, control of inhomogeneity and decrement of defects are crucial for promoting the mechanical performance of SiC fibers. A previous study [14] showed that a chemical gradient exists along the radial direction of SiC fibers, and the content of carbon (or the

---

[*] Corresponding authors.
E-mail addresses: cuilanwu@hnu.edu.cn (C. Wu), y.gou2012@hotmail.com (Y. Gou).

https://doi.org/10.1016/j.matchar.2018.09.041
Received 21 June 2018; Received in revised form 10 September 2018; Accepted 25 September 2018

C/Si ratio) increases from the surface to the core of the fibers, suggesting a generally existed inhomogeneous phase distribution across the precursor-derived SiC fibers. Both a fully dense, stoichiometric region and a porous, carbon-rich region are observed for the nearly stoichiometric polycrystalline SiC fibers [9,13]. However, the specific distribution of the stoichiometric and carbon-rich regions as well as defects in the cross-section of SiC fibers is still unknown. In addition, graphite exhibits various forms, including straight, turbostratic or cage-like [9,10,24], but the reason for the morphologies of graphite remains unclear. At the same time, although aluminum as a sintering aid plays a significant role in the PACS-derived fibers, the location of Al in the fibers has not been confirmed. Therefore, an understanding of fine and detailed microstructural and microchemical distribution of SiC fibers is becoming more and more important and urgent for further improvement of the mechanical and high-temperature performance of SiC fibers.

In the present work, a detailed study of the microstructural and microchemical distribution of the nearly stoichiometric polycrystalline SiC fiber is conducted by using scanning electron microscopy (SEM), transmission electron microscopy (TEM) equipped with energy-dispersive X-ray spectrometers (EDS) and first-principles calculations. One amorphous SiC fiber and another polycrystalline SiC fiber with non-stoichiometric composition are carefully chosen for systematically comparison of the composition, microstructure and properties with the nearly stoichiometric polycrystalline SiC fiber. In addition, the microstructural evolution under different thermal conditions is also analyzed.

2. Experimental and Calculation Procedures

2.1. Materials and Characterization Methods

Three typical PACS-derived SiC fibers fabricated with different sintering processes were used in the experiments. The tensile strength was obtained by the method in Ref. [19]. To measure the thermal stabilities of the fibers, they were heat-treated at high temperature for 1 h in argon or air and then cooled in the furnace. The sintering temperatures, composition, C/Si atomic ratios and the tensile strengths of these fibers are listed in Table 1. Fiber F-1 and fiber F-2 are non-stoichiometric SiC fibers derived from the same organic precursor at different sintering temperatures. Fiber F-3 is a near-stoichiometric SiC fiber. The fibers were prepared by using the procedure from our previous work [20,21]. The PACS precursors were used to prepare the three types of SiC fibers by following melt-spinning, curing, pyrolysis and final sintering. The fiber F-1 obtained from PACS precursor by sequentially melt-spinning at 300 °C under nitrogen, curing at 160 °C under air, and pyrolyzing at 1200 °C under nitrogen. When the fiber F-1 was further sintered at 1800 °C under argon, it produced the fiber F-2. The fabrication process of fiber F-3 was same as the F-2, but with a higher curing temperature of 180 °C.

The XRD measurements were carried out on a Rigaku SmartLab X-ray diffractometer with Cu-Kα radiation ($\lambda = 1.54$ Å). The surface and cross-sectional morphologies of SiC fibers were obtained from a JSM-6700F field emission SEM. TEM observations and electron diffraction spectra were performed by using a JEM-3010 microscope. High-resolution TEM (HRTEM) images, high-angle annular dark-field scanning TEM (HAADF-STEM) images, and elemental mapping were obtained from an FEI Tecnai F20 microscope equipped with EDS. Due to the large collection angle of HAADF detectors, the brightness in the obtained HAADF images is approximately proportional to Z^2 (where Z is the atomic number of atoms) [25–27]. Here, an FEI Helios NanoLab 600i focused ion beam (FIB) system was employed to prepare the cross-sectional sample for TEM observations. In order to reduce the damage of the high-energy ion beam, a thin platinum (Pt) protection layer was deposited on the fiber surface via electron beam, and then a thick Pt layer was deposited on the former Pt layer by ion beam. The specimens were firstly cut and milled by ion beam towards about 60 nm, and then were milled for several minutes at low voltage and low beam current to minimize the amorphous layer induced by ion beam damage.

2.2. Calculation Details of Phase Stability

Here, the phase stability measured by the formation enthalpies [28,29] of Al-doped β-SiC was obtained by using the Vienna Ab initio Simulation Package (VASP) code [30,31]. The projector augmented wave (PAW) method [32] was used to treat the interaction between ion and core electrons. Valence electrons were described using the generalized gradient approximation (GGA) with the Perdew, Burke and Ernzerhof (PBE) exchange–correlation function [33]. The convergence tests indicated that 600 eV was a sufficient cutoff energy for the PAW potential to obtain high precision in the current systems. Brillouin-zone gridding was performed using the Monkhorst-Pack method [34].

3. Results and Discussion

3.1. Microstructural Distribution of the SiC Fibers

Fig. 1 displays the XRD spectra for the three different SiC fibers. Fiber F-1 shows broadening diffraction peaks with low intensity, indicating rather low crystallinity. Hence, F-1 can be approximately regarded as an amorphous fiber. Unlike fiber F-1, fibers F-2 and F-3 are both highly crystallized and mainly consist of β-SiC crystals with twins and stacking faults (SFs). In addition, a small amount of graphite was found in fiber F-3 but cannot be found in fiber F-2. This should be attributed to the crystallinity difference of graphite between fiber F-2 and fiber F-3, which will be discussed in detail later by TEM. Besides, the diffraction peak intensity of fiber F-3 is stronger than fiber F-2 (as shown in Fig. 1), suggesting higher crystallinity of β-SiC of fiber F-3.

As shown in Fig. 2, these fibers all have clean surfaces and uniform diameters. Enlarged images demonstrate the dense surfaces of fibers F-1 (Fig. 2b) and F-2 (Fig. 2d), while a few pores with a size of 50–150 nm are found on the surface of fiber F-3 (Fig. 2f). The pores, whose sizes are comparable to that of the SiC grains, can likely be attributed to the gas release induced fall-off of the SiC grains during sintering [22]. Since pores have negative effects on the mechanical properties of the fibers, fiber F-3 exhibits a slightly lower tensile strength than the present commercial fibers (3.0 GPa). No special feature is observed on the surface of fiber F-1 as it mainly consists of amorphous phase due to the low pyrolysis temperature (1200 °C). When the sintering temperature increases up to 1800 °C, SiC grains grow, as observed on the surface of fiber F-2. However, unlike fiber F-3, in which the grain boundaries are clean and clearly distinguishable, something different surrounds the SiC grains in fiber F-2, which will be discussed later.

The fracture morphologies of the SiC fibers are revealed in Fig. 3. Fiber F-1 shows a smooth fracture surface, but rough fracture surfaces

Table 1
Sintering temperatures, composition and properties of three typical SiC fibers.

Fiber	Temperature (°C)	Si content (wt%)	C content (wt%)	O content (wt%)	C/Si atomic ratio	Al content (wt%)	Tensile strength (GPa)	Elastic modulus (GPa)
F-1	1200	54.60	35.83	8.62	1.53	< 1.0	1.5	177
F-2	1800	63.89	34.50	0.11	1.26	< 1.0	0.8	195
F-3	1800	67.05	31.05	0.08	1.09	< 1.0	2.5	315